Journal of Magnetic Resonance **153,** 7–14 (2001)
doi:10.1006/jmre.2001.2415, available online at http://www.idealibrary.com on IDEAL®

Enhanced EPR Sensitivity from a Ferroelectric Cavity Insert

Yuri E. Nesmelov, Jack T. Surek, and David D. Thomas[1]

Department of Biochemistry, University of Minnesota Medical School, Minneapolis, Minnesota 55455

E-mail: ddt@umn.edu

Received January 23, 2001; revised July 24, 2001; published online October 5, 2001

We report the development of a simple ferroelectric cavity insert that increases the electron paramagnetic resonance (EPR) sensitivity by an order of magnitude when a sample is placed within it. The insert is a hollow cylinder (length 4.8 mm, outside diameter 1.7 mm, inside diameter 0.6 mm) made from a single crystal of $KTaO_3$, which has a dielectric constant of 230 at X-band (9.5 GHz). Its outside dimensions were chosen to produce a resonant frequency in the X-band range, based on electromagnetic field modeling calculations. The insert increases the microwave magnetic field (H_1) at the center of the insert by a factor of 7.4 when placed in an X-band TM_{110} cavity. This increases the EPR signal for a small (volume 0.13 μL) unsaturated nitroxide spin label sample by a factor of 64 at constant microwave power, and by a factor of 9.8 at constant H_1. The insert does not significantly affect the cavity quality factor Q, indicating that this device simply redistributes the microwave fields within the cavity, focusing H_1 onto the sample inside the insert, thus increasing the filling factor. A similar signal enhancement is obtained in the TM_{110} and TE_{102} cavities, and when the insert is oriented either vertically (parallel to the microwave field) or horizontally (parallel to the DC magnetic field) in the TM_{110} cavity. This order-of-magnitude sensitivity enhancement allows EPR spectroscopy to be performed in conventional high-Q cavities on small EPR samples previously only measurable in loop–gap or dielectric resonators. This is of particular importance for small samples of spin-labeled biomolecules.

Key Words: **electron paramagnetic resonance; ferroelectric; $KTaO_3$; cavity insert; muscle fiber.**

INTRODUCTION

Improving the sensitivity (signal-to-noise ratio for a given sample) in EPR is particularly important for studying biological samples, which are often available only in limited amounts, particularly in analysis of protein mutants or single cells. In current EPR spectrometers, noise is constant and limited by the detector over a wide range of incident microwave power. Therefore, the goal of sensitivity enhancement is reduced to the task of increasing the signal intensity S at a constant number of spins. For the common case of a detector with a linear response, the signal intensity S is given by (*1*)

$$S \propto \eta\, Q\, P^{1/2}, \qquad [1]$$

where η is the filling factor, Q is the unloaded quality factor of the cavity, and P is the incident microwave power. In most EPR experiments, the power is adjusted to maximize signal intensity in the absence of saturation. For each sample, this condition is achieved at a characteristic value of the microwave magnetic field amplitude H_1 at the sample, which is proportional to the square root of the incident power making the practical definition of sensitivity (relative signal at the optimal H_1 and constant number of spins)

$$S \propto \eta\, Q H_1. \qquad [2]$$

For most spectrometers and samples, it is easy to obtain a value of P high enough to achieve the optimal H_1 value. Therefore, optimizing sensitivity is usually a matter of increasing Q or η. Most modern EPR cavities have been designed for optimally high Q, so our goal is to start with a commercial high-Q cavity and to increase the filling factor η, which is given by (*1*)

$$\eta = \left(V_s\langle H_1^2\rangle_s\right)/\left(V_c\langle H_1^2\rangle_c\right), \qquad [3]$$

where V_s and V_c are volumes of the sample and cavity, and $\langle H_1^2\rangle_s$ and $\langle H_1^2\rangle_c$ are the mean square microwave magnetic field values in the sample and cavity, respectively.

For the rectangular TE_{102} cavity ($V_c \cong 10$ cm^3), the filling factor is about $2\,V_s/V_c = 2 \times 10^{-4}$ for a 1-μL "point" sample and $V_s/V_c \cong 2 \times 10^{-3}$ for an optimal aqueous line sample (20 μL) (*1*). Noncavity resonators, such as loop–gap resonators (LGRs) or dielectric resonators (DRs), typically have filling factors 50–100 times greater than that of a TE_{102} cavity (*3, 5*), but a number of disadvantages limit the application of these devices. For example, a LGR has a low Q and can be difficult to tune. Its absorption spectrum is often distorted by a dispersion component, due to errors of phasing in the reference arm of the microwave bridge (*6*). Furthermore, most X-band EPR users already use cavities for biochemical measurements.

[1] To whom correspondence should be addressed.

1090-7807/01 $35.00

Buying an LGR or DR can be as expensive as buying a new cavity because they can be difficult to manufacture (*3, 4*). Therefore, it is desirable to devise a means to increase the filling factor of a conventional resonant cavity.

It is possible to increase the filling factor by increasing the volume of the sample, but for aqueous samples this approach is severely limited by dissipative losses that can degrade Q and thus decrease S (Eq. [1]). Therefore, our goal is to redistribute H_1 so that it is concentrated at the sample. There have been previous attempts to concentrate the H_1 field at the sample by insertion of a resonant structure into a cavity, e.g., using a folded half-wave resonator (*7*) or a LGR (*8*). Even a quartz dewar (dielectric insert) increases H_1 at the sample through such a perturbation. For a dielectric or ferroelectric insert, H_1 at the sample increases in proportion to the square root of the dielectric constant (ε) of the insert material (*1*). This led to experimentation with low-loss microwave ceramics in resonators for EPR, with dielectric constants of about 30 (*4*) as well as low-loss ferroelectric materials that have constants of 100 to 300 (*9, 10*).

In the present study, we have investigated a crystalline ferroelectric, $KTaO_3$, for use as a hollow cylindrical insert in an X-band microwave cavity. Cylinder dimensions were calculated with mode matching (*11–14*) to produce an insert with an X-band resonant frequency. The microwave magnetic field H_1 at the sample in the cavity with and without the insert was measured from the signals of EPR samples with known saturation properties, and the effect of the insert on EPR signal intensity was determined for samples of free spin-label solutions, spin-labeled lipids, and muscle fibers.

METHODS

Theoretical

Our goal was to fabricate an insert with a bore for the introduction of samples. We also wanted an insert with cylindrical symmetry, to ensure its excitability by the $TE_{01\delta}$ mode and to facilitate the calculation of microwave fields. Therefore, as a first approximation we designed the insert as a solid cylinder with an X-band resonant frequency. We used radial mode matching to compute the resonant frequency of the lowest order TE mode (*11*).

The computation starts with the well-known Helmholtz vector equation (*12–14*)

$$(1/r)d(r(d\Psi/dr))/dr - (m^2/r^2)\Psi + d^2\Psi/dz^2 + k_0^2\varepsilon\Psi = 0, \qquad [4]$$

where wavenumber $k_0 = 2\pi/\lambda$ in air and $k_0\varepsilon^{1/2}$ in the cylinder insert. Here $m = 0$ because of axial symmetry. Equation [4] is solved separately for regions I and II (Fig. 1) by separation of variables

$$\Psi = R(r)Z(z). \qquad [5]$$

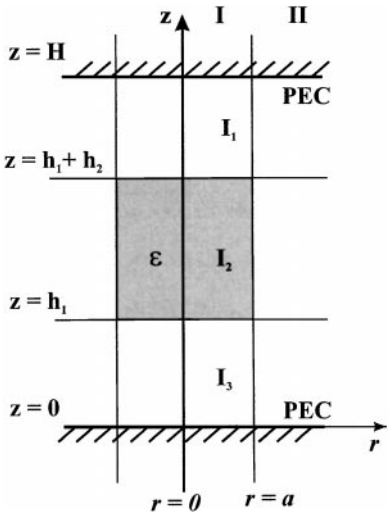

FIG. 1. Model of shielded solid cylindrical dielectric resonator. PEC is a perfect electric conductor.

We assume that most of the energy is stored in the insert and the microwave field decays exponentially in region II. Then, using Eq. [4] in region I,

$$(1/r)d(r(dR_1(r)/dr))/dr + p^2R_1(r) = 0 \qquad [6]$$

$$d^2Z_1(z)/dz^2 + v^2Z_1(z) = 0, \qquad [7]$$

and in region II,

$$(1/r)d(r(dR_2(r)/dr))/dr - q^2R_2(r) = 0 \qquad [8]$$

$$d^2Z_2(z)/dz^2 + t^2Z_2(z) = 0, \qquad [9]$$

where p^2 and q^2 are the eigenvalues and $v^2 = k_0^2\varepsilon - p^2$, $t^2 = k_0^2 + q^2$.

The solution of Eq. [6] is a Bessel function $R_1(r) = J_0(pr)$ (we reject the solution $R_1(r) = Y_0(pr)$ because it becomes infinite at $r = 0$) as well as the solution of Eq. [8], $R_2(r) = K_0(qr)$.

The solution of Eq. [9] is $Z_2(z) = \sin(tz)/t$ (we reject the solution $Z_2(z) = \cos(tz)$ because $\Psi = 0$ at $z = 0$ and $z = H$ due to boundary conditions). Then, because of boundary conditions $\Psi = 0$ at $z = 0$ and $z = H$, $tH = \pi n$ or $t = \pi n/H$ and $n = 1$ because we consider only the first low TE mode.

The solution of Eq. [7] for region I is more complicated because of layers with different dielectric constants of air and the insert and eigenfunction Z_1 can be constructed as (*12*)

—in layer I_1,

$$Z_{11}(z) = \sin(v_1 z)/v_1, \qquad [10]$$

—in layer I_2,

$$Z_{12}(z) = B\sin(v_2(z - h_1))/v_2 + C\cos(v_2(z - h_1)), \qquad [11]$$

—in layer I_3,

$$Z_{13}(z) = D\sin(v_1(z-H))/v_1, \qquad [12]$$

where $B = \cos(v_1h_1)$, $C = (\sin(v_1h_1)/v_1)$, and $D = \cos(v_2h_2) - (v_2/v_1)(\sin(v_1h_1)/\cos(v_1h_1))\sin(v_2h_2)$. The insert is in the center of a cavity, which means that $h_1 = H-(h_1+h_2)$. The continuity of tangential fields of region I requires that $Z_{11} = Z_{12}$ at $z = h_1$, $Z_{12} = Z_{13}$ at $z = h_1 + h_2$, and $dZ_{11}/dz = dZ_{12}/dz$ at $z = h_1$, $dZ_{12}/dz = dZ_{13}/dz$ at $z = h_1 + h_2$. Then, from Eqs. [10]–[12],

$$2(v_2/v_1)tg(v_1h_1) + tg(v_2h_2)\{1-(v_2/v_1)^2tg^2(v_1h_1)\} = 0. \qquad [13]$$

A fundamental property of these solutions is that the eigenvalues p^2 are less than $k_0^2\varepsilon$ (*13*, *14*). We need to find only the first eigenvalue because we compute the resonant frequency for only the first low TE mode.

When eigenvalues p^2 and q^2 are found, the resonant frequency is found by matching the tangential microwave fields at the boundary between regions I and II. The fields $H_\phi = E_z = E_r = 0$ (*13*) and tangential microwave fields can be expressed as

$$H_z = -\left\{d^2\Psi/dz^2 + k_0^2\varepsilon\Psi\right\},$$
$$E_\phi = d\Psi/dr. \qquad [14]$$

Regions I and II is boundary conditions

$$H_z^{\mathrm{I}} = H_z^{\mathrm{II}} \text{ at } r = a,$$
$$E_\phi^{\mathrm{I}} = E_\phi^{\mathrm{II}} \text{ at } r = a$$

give the equation

$$J_0(pa)/J_1(pa) = -(q/p)\,K_0(qa)/K_1(qa), \qquad [15]$$

which must be solved to determine the frequency of resonance.

The resonance frequency of our cavity is $\nu = 9.316$ GHz, and the dimensions of the insert calculated by this method were $h_2 = 3.85$ mm and $2a = 1.76$ mm at this frequency. The relative dielectric constant of the $KTaO_3$ crystal was assumed to be $\varepsilon = 230$ at 10 GHz (*15*). A hole was drilled down the axis for sample loading, assuming that this does not affect the resonance frequency substantially. We guessed that this perturbation could be compensated with a slight increase in value of the insert height h_2. The final dimensions were 4.8 mm in height with 1.76 mm as outside diameter and 0.6 mm as inside diameter. The value $2a = 1.76$ mm is an average value; the insert has a slightly conical shape, with a difference of 0.04 mm between the diameters of the ends. The axis of the insert was made parallel to the [100] axis of a $KTaO_3$ crystal (although the dielectric constant is specified to be isotropic for this crystal). The insert was centered with its axis perpendicular to the external magnetic field in the TE and TM cavities and parallel to the external magnetic field for the transverse orientation for the TM cavity.

Experimental

EPR experiments were performed with a Bruker EleXsys E500 spectrometer (Bruker Instruments Inc., Billerica, MA), using either (1) a TE_{102} cavity (model 4102 ST; Bruker Instruments Inc.) with a quartz dewar, (2) a TM_{110} cavity (model 4103 TM; Bruker Instruments Inc.) with no dewar, or (3) a loop–gap resonator (Medical Advances, Milwaukee, WI) with an external dewar. In all cases the axis of the sample tube and the insert was placed vertically, perpendicular to the DC magnetic field H_0 and parallel to the microwave magnetic field H_1, except in the case of the TM cavity, which was modified to place the axis either parallel or perpendicular to the DC magnetic field (*16*). The temperature was controlled at 23°C using a nitrogen gas-flow temperature controller, and monitored with a digital thermometer using a Sensortek (Clifton, NJ) IT-21 thermocouple microprobe inserted into the top of the sample capillary, such that it did not affect the EPR signal. The spectra were acquired using 100 kHz field modulation. Peak-to-peak modulation amplitude was 0.01 G for measurements of the distribution of signal intensity vs position along the cavity axis with a BDPA point sample, 0.5 G at measurement of saturation rollover curves, 2 G at measurement of lipid sample, and 3 G at muscle fiber sample measurements. All investigated samples were loaded into fused quartz round capillaries with 0.4 mm ID, 0.55 mm OD (Vitro Dynamics Inc., Rockaway, NJ). Crystals of $KTaO_3$ were obtained as a gift from Dr. L. A. Boatner (Oak Ridge National Laboratory, TN). The quality factors Q of the unloaded cavity with and without the insert were measured with an HP 8510C Network Analyzer and found as the ratio of resonance frequency to dip linewidth, measured at −3 dB from the baseline.

The microwave magnetic field amplitude H_1 at the sample was calibrated by measuring the half-saturation power $P(1/2)$ of 0.9 mM deoxygenated peroxylamine disulfonate (PADS) in 10 mM K_2CO_3 aqueous solution (*2*). The relationship between H_1 and incident power is given by the equation

$$H_1 = C\,P^{1/2}. \qquad [16]$$

The constant C incorporates the effect of quality factor (Q) and filling factor (η). TE_{102} and TM_{110} cavities typically have $C \approx 1$ G/W$^{1/2}$, while LGRs and DRs typically have $C \approx 4$–5 G/W$^{1/2}$. To determine power at half-saturation, the dependence of signal intensity on the square root of incident power (saturation rollover curve) was obtained as shown in Fig. 2. H_1 at half-saturation for PADS is 0.1067 G (*2*); the ratio of this H_1 to the square root of the corresponding incident power gives C. Knowing C allows the field H_1 at the sample to be related to the incident power. The constants C for TE_{102} with dewar and for TM_{110} are shown in Table 1 in the column marked as C_0.

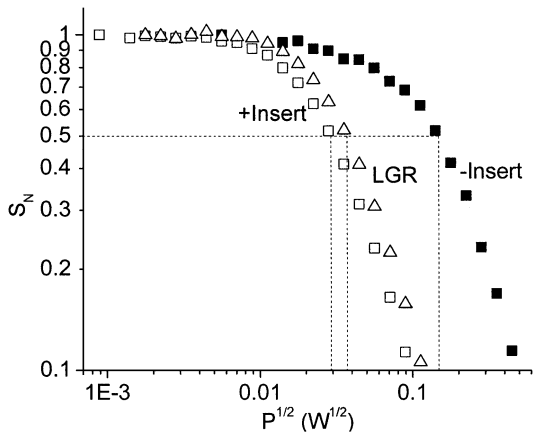

FIG. 2. Saturation rollover curves for 100 μM IASL aqueous solution for the TE_{102} cavity without (filled squares) and with the insert (open squares) and the LGR (open triangles). P is the incident microwave power. S_N is the signal intensity normalized so that a value of 1 indicates no saturation (signal proportional to $P^{1/2}$); i.e., $S_N = (S(P)/P^{1/2})/(S(P_0)/P_0^{1/2})$, where P_0 is a nonsaturating power.

For simplicity, H_1 calibrations at the sample for cavities with and without the insert and for the LGR were made with a 100 μM IASL aqueous solution. The saturation behavior of a sample that has IASL free in solution is determined solely by the relaxation properties of IASL and should be the same in different resonators, with and without the insert. Saturation rollover curves for the TM_{110} cavity with and without the insert in perpendicular and parallel orientations and for the TE_{102} cavity with and without the insert in perpendicular orientation were obtained. Constants C for the different cases were then determined and are shown in the Table 1. Figure 2 shows examples of saturation rollover curves of 0.2 μL of 100 μM IASL aqueous solution in the TE_{102} cavity with and without the insert and in the LGR.

The following reagents and solutions were used in this study: peroxylamine disulfonate (PADS), free radical BDPA complex with benzene (α,γ-bisdisdiphenylene-β-phenylallyl), 4-(2-iodoacetamido)-2,2,6,6-tetramethyl-1-piperidinyloxy (IASL), TEMPO, and 4′,4,-dimethyloxazolidine-5-oxyl derivative of stearic acid (5-SASL) (all Aldrich Chemicals Co., Milwaukee, WI), and dioleoylphosphatidylcholine (DOPC) lipids (Avanti Polar Lipids, Alabaster, AL).

Lipid sample preparation. DOPC and 5-SASL (100/1) were mixed in chloroform, and the solvent was removed under a stream of nitrogen gas that left the lipid sample deposited as a thin layer at the bottom of a glass test tube. Chloroform traces were removed under vacuum. The dried lipid sample was then rehydrated with MOPS buffer (pH 7.0), pipetted into a capillary flame-sealed on one end, and then concentrated by centrifuging at 100,000 rpm for 30 min. After removing the excess liquid, the sample length was 1.7 mm; the quantity of 5-SASL in the sample was 0.4 nmoles.

Muscle sample preparation. Psoas muscle from New Zealand white rabbits was dissected, glycerinated, and spin labeled specifically at Cys 707 (SH1) with IASL in rigor buffer (130 mM potassium propionate, 20 mM MOPS, 1 mM EDTA, 2 mM $MgCl_2$, 1 mM NaN_3) as described elsewhere (*17*). After labeling, the fiber bundles were washed in a mixture of 50% glycerol and 50% rigor buffer. A muscle fiber bundle with diameter 0.15 mm and length 4 mm was placed in a capillary and held isometrically by suture tied to the bundle ends. The capillary was filled with a mixture of 50% glycerol and 50% rigor buffer and sealed with Critoseal at both ends.

RESULTS

Introducing the insert into the cavity increased the EPR signal substantially, without increasing the noise. For example, the signal intensity from an unsaturated point sample of BDPA, placed in the center of a TE cavity, was increased by a factor of 45 (Fig. 3). This factor was even greater for a TM cavity: 80 if the insert was perpendicular to the DC field (Fig. 4) and 67 if the

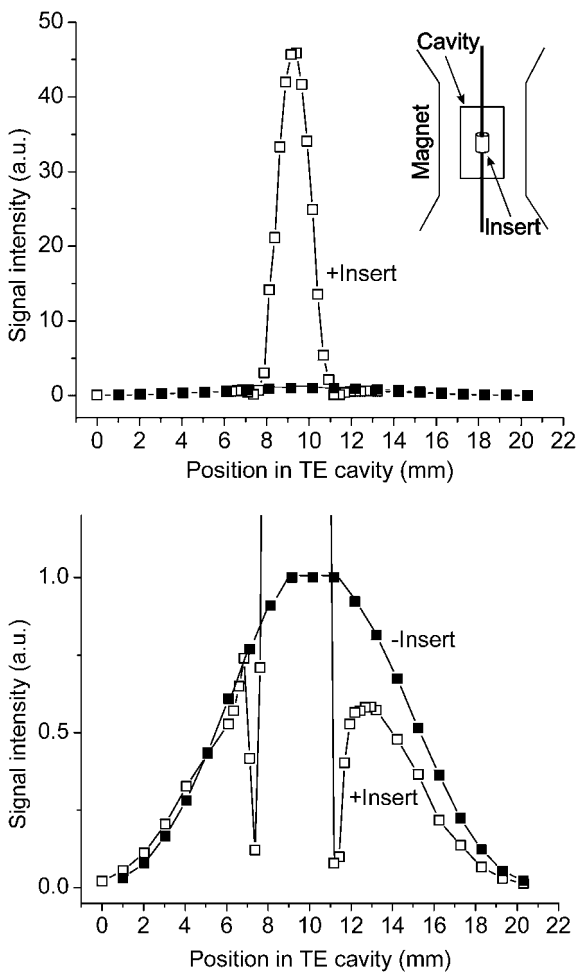

FIG. 3. Distribution of signal intensity of a point BDPA sample along the vertical axis (perpendicular to the DC magnetic field) of the TE_{102} cavity without (filled squares) and with the insert (open squares).

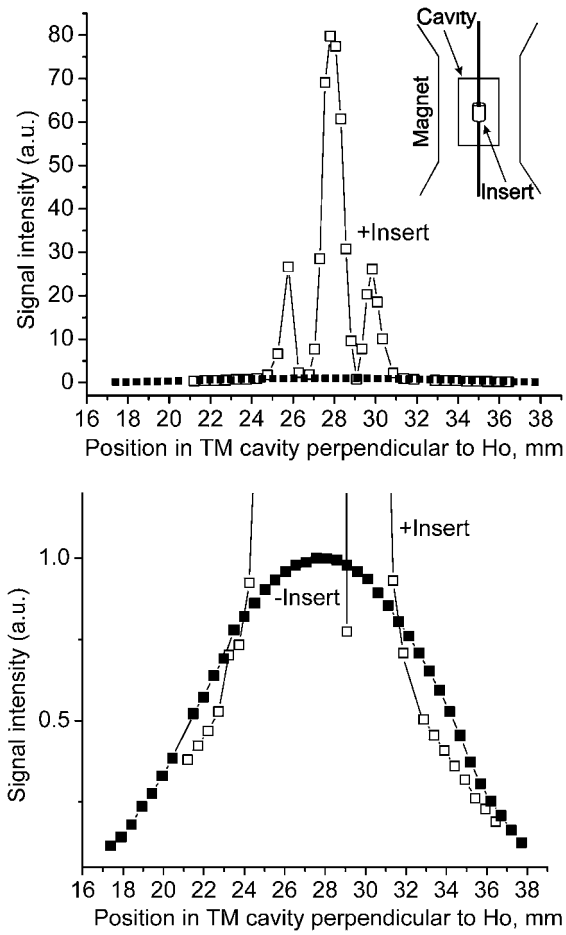

FIG. 4. Distribution of signal intensity of a point BDPA sample along the vertical axis (perpendicular to the DC magnetic field) of the TM_{110} cavity, without (filled squares) and with the insert (open squares).

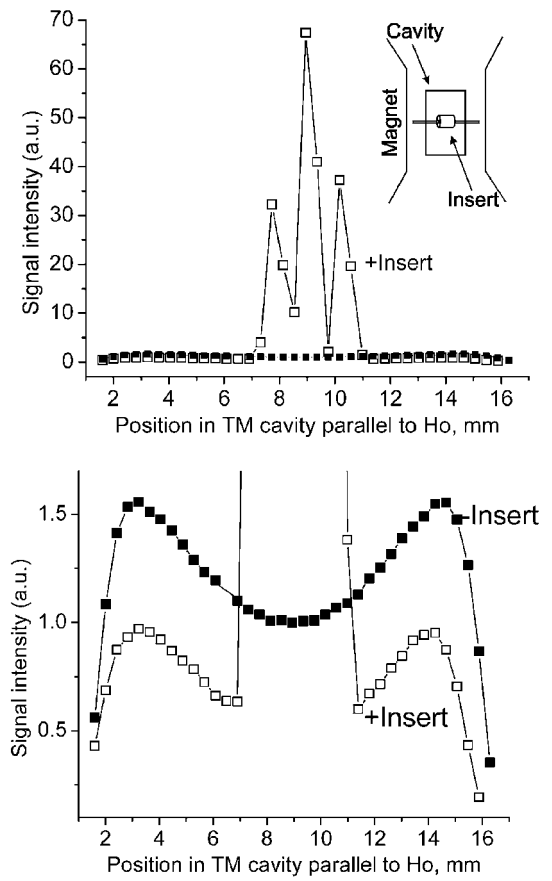

FIG. 5. Distribution of signal intensity of point BDPA sample along the horizontal axis (parallel to DC magnetic field) of the TM_{110} cavity, without (filled squares) and with the insert (open squares).

insert was parallel to the DC field (Fig. 5). Figures 3, 4, and 5 show the dependence of signal intensity on the position of this point sample along the cavity axis, normalized to the signal at the center of the cavity in the absence of the insert. The asymmetry in Figs. 3, 4, and 5 is probably due to imprecise centering of the insert in the cavity or imperfection in its cylindrical shape (see Introduction).

Figure 6 shows the spectrum of 0.6 μL of 10 μM TEMPO spin label in a cavity with the insert (raw), a baseline (spectrum of cavity with the insert and with the same amount of distilled water replacing the TEMPO), and the spectrum resulting from subtraction of the baseline from the TEMPO spectrum. The baseline of the cavity with the insert shows a weak EPR line with $g = 2.004$ and a peak-to-peak linewidth of 12 G. The EPR signal of the insert probably corresponds to trace Fe^{3+} ions (*18*, *19*).

A comparison of the performance of the TE cavity with insert and the LGR for 0.2 μL of 10 μM aqueous TEMPO at the same incident power shows that the LGR produces a more intense signal; the ratio of signal intensities of the same sample in the LGR and in the TE cavity with the insert is 2.2.

We found a shift in the frequency of resonance when the insert is placed in the cavity. For the TE cavity, the resonance frequency changed from 9.316 to 9.361 GHz, for the TM cavity from 9.801 to 9.809 and 9.804 GHz in the perpendicular and parallel insert orientations, respectively.

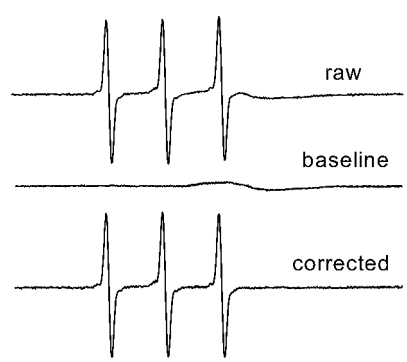

FIG. 6. EPR spectra for baseline subtraction acquired for 0.6 μL of 10 μM TEMPO aqueous solution. Experimental conditions: gain 80 dB (2e5), $P = 0.63$ mW, time constant 41 ms, sweep 120 G/42 s, 25 scans acquired for each trace.

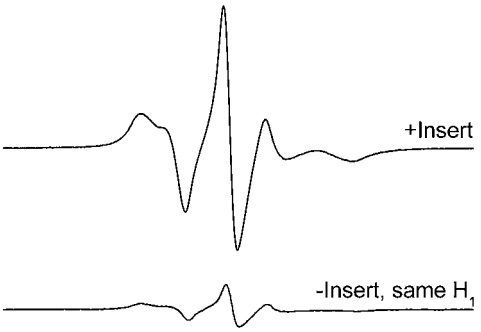

FIG. 7. EPR spectra acquired for a lipid sample: fatty acid spin label 5-SASL in DOPC lipids. The quantity of 5-SASL in the sample is approx. 0.4 nmoles. In the TE cavity with the insert, $P = 0.63$ mW, $H_1 = 123$ mG (top). In the TE cavity without the insert, $P = 15.94$ mW, $H_1 = 121$ mG (bottom). Sample length, 2.2 mm; volume, 0.3 μL. Experimental conditions: gain 80 dB (2e5), time constant 41 ms, sweep 110 G/42 s, 30 scans acquired for each trace.

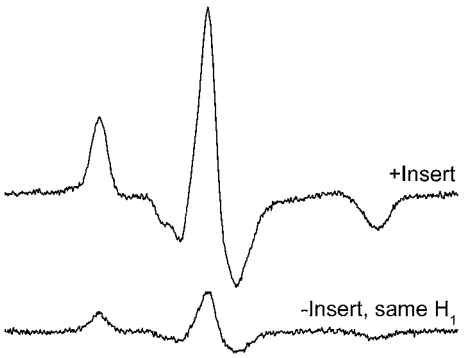

FIG. 9. EPR spectra recorded for a muscle fiber bundle in parallel orientation spin labeled at Cys707 of myosin head (SH1) by IASL. In the TM cavity with the insert, $P = 0.63$ mW, $H_1 = 146$ mG, baseline subtracted (top). In the TM cavity without the insert, $P = 31.81$ mW, $H_1 = 139$ mG (bottom). Experimental conditions: gain 80 dB (2e5), time constant 41 ms, sweep 120 G/42 s, 20 scans acquired for each trace.

We observed dramatic amplifications of EPR spectra without significant distortion when the ferroelectric insert bore was loaded with lossy aqueous samples in all orientations. This is strong evidence that the microwave magnetic and electric fields remain spatially well separated between the insert bore and sidewall, respectively. We also found no shift in resonance frequency between an empty bore and one with a lossy sample loaded in all orientations. This means the power loss due to the interaction of the microwave electric field with the aqueous (muscle fiber) sample is small.

Enhancement of EPR signals of biological samples by the insert, at constant H_1, is shown in Figs. 7, 8, and 9. Figure 7 shows the EPR spectra of 5-SASL in DOPC lipid bilayers in the TE cavity. Figures 8 and 9 show the EPR spectra of a muscle fiber bundle perpendicular and parallel to the external magnetic field mounted in the TM cavity. The enhancement for fatty acid spin label in lipid bilayers in the TE cavity is 6.4 (Fig. 7). The enhancement for a spin-labeled muscle fiber handle in the TM cavity is 4.7 when the insert and fiber are placed perpendicular to DC field and 4.5 when the orientation of the insert and fiber are parallel to the DC field.

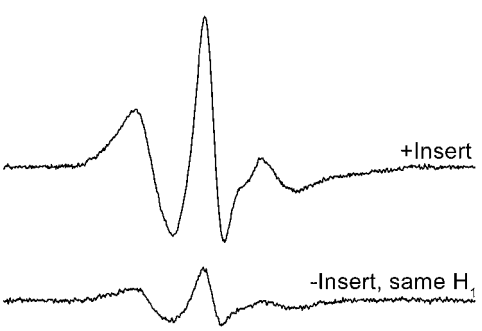

FIG. 8. EPR spectra recorded for a muscle fiber bundle in perpendicular orientation spin labeled at Cys707 of myosin head (SH1) by IASL. In the TM cavity with the insert, $P = 0.63$ mW, $H_1 = 138$ mG, baseline subtracted (top). In the TM cavity without the insert, $P = 31.81$ mW, $H_1 = 139$ mG (bottom). Experimental conditions: gain 80 dB (2e5), time constant 41 ms, sweep 120 G/42 s, 20 scans acquired for each trace.

Table 1 illustrates the effect of the insert on H_1 and signal intensity for various samples and cavities. The first and second columns give values of conversion factor C_0 for the cavity without the insert and C for the cavity with the insert, where C is the ratio of H_1 and $P^{1/2}$ (Eq. [16]). The third column presents the ratio of conversion factors C/C_0, which is the ratio of H_1 at the sample in the cavity with and without the insert at the same incident power. The last four columns show ratios of signal intensities of different samples in cavities with and without the insert at the same H_1 or at the same incident power, under unsaturated conditions. Samples were centered simultaneously in the cavity and the insert. The point sample was a tiny piece of BDPA. The aqueous samples were 1 mM TEMPO, 0.2 μL ($l = 1.7$ mm) for the TE cavity and 0.13 μL ($l = 1$ mm) for the TM cavity. The different volumes were chosen to completely fill only the central part of the microwave magnetic field distribution found throughout the insert (see Figs. 3–5). Column eight shows ratios of integral intensity of signals of the muscle fiber bundle sample in the cavity with and without the insert at the same H_1 at the sample.

DISCUSSION

Enhancement of Signal Intensity and Filling Factor of a Cavity with the Insert

As indicated in the discussion of Eq. [1] in the Introduction, EPR sensitivity for a given sample is proportional to the quality factor Q and the filling factor η. We found that the ferroelectric insert had no significant effect on Q, so the improvement in signal intensity with the insert is found to be directly proportional to the increased filling factor

$$(S/S_0)_P \propto (\eta/\eta_0), \qquad [17]$$

TABLE 1

Cavity/insert orientation	C_0[a] $(G/\sqrt{W})$	C[b] $(G/\sqrt{W})$	C/C_0[c]	Signal intensity ratio[d]: Point sample[e], same power $(S/S_0)_P$	Aqueous sample[f]: Same power $(S/S_0)_P$	Aqueous sample[f]: Same H_1 $(S/S_0)_{H_1}$	Muscle fiber[g], same H_1 $(S/S_0)_{H_1}$
TE	0.96	4.7	4.9	45	34[h]	7[h]	
TM/perpendicular	0.78	5.8	7.4	80	64[i]	9.8[i]	4.7
TM/parallel	0.78	5.5	7	67	56[i]	8.5[i]	4.5

[a] Cavity conversion factor ($C = H_1/P^{1/2}$) without insert.
[b] C with insert.
[c] Increase of H_1 at the sample in cavity with the insert.
[d] Ratio of signal intensities of sample in cavity with and without insert.
[e] BDPA.
[f] 1 mM TEMPO aqueous solution.
[g] Four millimeter muscle fiber bundle labeled by IASL at Cys707 of SH1.
[h] $V = 0.2\,\mu$L, $l = 1.7$ mm.
[i] $V = 0.13\,\mu$L, $l = 1$ mm.

where 0 indicates the absence of the insert. Both signals S and S_0 are measured under unsaturated conditions. For fixed volumes of sample and cavity, and considering Eq. [3], we conclude that the improvement of signal intensity reflects the redistribution of the microwave field H_1 in the cavity by the insert, such that more of the available magnetic field H_1 is focused on the sample.

The difference in the signal intensities for a point sample and for an aqueous sample in Table 1 can be explained by the variation in microwave magnetic field strength along the axis of the linear sample covered by the insert compared with a constant and maximal field H_1 for the point sample in the center of the insert (Figs. 3–5). Thus the peak field H_1 detected with a point sample in the center of the insert is larger than the average field H_1 throughout the insert for a 1.7-mm (TE) and 1-mm (TM) long line sample. Also, a 4-mm muscle fiber sample shows an even lower signal intensity ratio, as it extends a significant length from the center of the insert, where H_1 has a maximum value.

According to Eq. [17], the signal intensity ratio is proportional to the ratio of filling factors for the cavity with and without the insert. Then, from Eq. [16],

$$(S/S_0)_{H_1} \propto (\eta/\eta_0)(C_0/C) = (S/S_0)_P(C_0/C), \qquad [18]$$

where $(S/S_0)_{H_1}$ is the signal intensity ratio at the same H_1, and $(S/S_0)_P$ is the signal intensity ratio at the same incident power. This equation can be tested precisely for the aqueous sample, since it is for this sample that the effective H_1 value is accurately calibrated. The data in Table 1 are in excellent agreement with Eq. [18] for the TE cavity (calculated $(S/S_0)_{H_1}$ is $34 \cdot (4.9)^{-1} = 6.9$, observed is 7.0), agreement is also good for TM/perpendicular (calculated $(S/S_0)_{H_1}$ is $64 \cdot (7.4)^{-1} = 8.7$, observed is 9.8), and for the TM/parallel (calculated $(S/S_0)_{H_1}$ is $56 \cdot (7)^{-1} = 8.0$, observed is 8.5). The small deviations are probably due to the 1-dB precision of the power setting, which limits the ability to achieve precisely the same H_1 for different C values, to nonuniform H_1 over the finite length of the sample, and/or to imprecise positioning of the sample in the center of the cavity.

The observed dramatic improvement of H_1 and signal intensity at the sample shows that there is a strong distributed coupling (*8*) between the insert and the cavity. In the frequency range from 9.1 to 9.9 GHz, only one resonance is observed, confirming the strong coupling of the insert to the cavity.

In the presence of the insert, there are two sharp minima of signal intensity in Figs. 3–5. For the TE cavity, the distance between these minima is 3.9 mm, which is in good agreement with the length of the resonator, as calculated from the solid cylindrical resonator model (3.85 mm). In a cylindrical insert the microwave magnetic field measured along the axis should have a maximum value in the center and minimum values at the ends, reflecting the boundary conditions. Thus the minima of signal intensity can be explained as nodes of a standing wave formed in the insert. This agreement between the model of a solid cylindrical resonator of $KTaO_3$ and the real cylindrical insert, which has an axial hole, confirms that the hole does not change the resonance conditions of the insert in cavity very much.

Performance of a Cavity with the Insert vs a Loop–Gap Resonator

The strengths of a LGR are a much greater filling factor η and much higher C_0 (i.e., $H_1/P^{1/2}$), compared with those of a cavity. The LGR increases H_1 by a factor of 8.2 compared to a cavity for the same incident power (*3*). For a 1-μL sample in a capillary with 0.6 mm ID, the filling factor η is about 0.29 in a LGR (*20*), compared with 2×10^{-4} in a TE_{102} cavity (*1*). This high value of the filling factor more than compensates for the low-quality factor Q of the LGR (600–800, compared with

2000–5000 for a cavity) and thus accounts for the improvement of EPR signal in the LGR in comparison with that in cavity. However, the low-quality factor of the LGR results in errors in phasing of the microwave bridge, which can lead to admixture of a dispersion component to the absorption EPR spectrum, thus distorting the spectrum. The low Q can also cause difficulties in tuning of the LGR, especially at high incident power (>10 mW). These problems are not observed for a cavity with the insert, since Q remains high.

Figure 2 shows that the cavity with the insert produces approximately the same H_1 at the sample as the LGR. The experimental comparison shows that for the same sample and the same incident power, the LGR produces about a twice as strong signal as the TE_{102} cavity with the insert. On the basis of Eq. [1], we conclude that the LGR still has a better filling factor than the cavity with the insert. However, it is likely that optimization of insert material and geometry in the future will produce an insert that matches or exceeds an LGR in sensitivity.

CONCLUSIONS

Introduction of a cylindrical $KTaO_3$ insert into an EPR cavity leads to a substantial increase in signal magnitude, due to a redistribution of the microwave electromagnetic field within the cavity, which increases the filling factor and the value of the microwave magnetic field at the sample, without significantly affecting the quality factor (Q) of the cavity. The resulting increase in signal magnitude for an unsaturated aqueous sample, using a commercial TM cavity, is a factor of 80 at constant incident microwave power and a factor of 9.8 at constant H_1. The insert is remarkably versatile and should provide a substantial sensitivity enhancement for a small aqueous sample for virtually any X-band EPR cavity and sample orientation.

ACKNOWLEDGMENTS

This work was supported by grants to D.D.T. from NIH (AR32961, GM27906), the Muscular Dystrophy Association, and the Minnesota Supercomputing Institute. We thank Dr. L. A. Boatner of Oak Ridge National Laboratory, TN, for the gift of the $KTaO_3$ crystals, Dr. A. Gopinath and Mr. D. Olson for assistance in measuring cavity Q, Ms. L. LaConte for a sample of spin-labeled muscle fibers, and Ms R. Bennett for helpful discussions.

REFERENCES

1. C. P. Poole, Jr., "Electron Spin Resonance," Dover, Mineola, NY (1996).
2. R. T. Weber and A. A. Heiss, Bruker ESP 300E EPR spectrometer user's manual (1992).
3. W. Froncisz and J. S. Hyde, The loop-gap resonator: A new microwave lumped circuit ESR sample structure, *J. Magn. Reson.* **47,** 515–521 (1982).
4. A. Sienkiewicz, M. Jaworski, B. G. Smith, P. G. Fajer, and C. P. Scholes, Dielectric resonator-based side-access probe for muscle fiber EPR study, *J. Magn. Reson.* **143,** 144–152 (2000), doi:10.1006/jmre.1999.1986.
5. M. Jaworski, A. Sienkiewicz, and C. P. Scholes, Double-stacked dielectric resonator for sensitive EPR measurements, *J. Magn. Reson.* **124,** 87–96 (1997).
6. B. H. Robinson, C. Mailer, and A. W. Reese, Linewidth analysis of spin labels in liquids, *J. Magn. Reson.* **138,** 199–209 (1999), doi:10.1006/jmre.1999.1737.
7. C. P. Lin, M. K. Bowman, and J. R. Norris, A folded half-wave resonator for ESR spectroscopy, *J. Magn. Reson.* **65,** 369–374 (1985).
8. J. R. Anderson, R. A. Venters, M. K. Bowman, A. E. True, and B. M. Hoffman, ESR and ENDOR applications of loop-gap resonators with distributed circuit coupling, *J. Magn. Reson.* **65,** 165–168 (1985).
9. I. N. Geifman and I. S. Golovina, Improvement of EPR sensitivity by use of a ferroelectric resonator–TE_{011} structure, 41st Rocky Mountain Conference on Analytical Chemistry, Abstract Book, p. 54, Denver, CO (1999).
10. O. G. Vendik, L. T. Ter-Martirosyan, and S. P. Zubko, Microwave losses in incipient ferroelectrics as functions of the temperature and the biasing field, *J. Appl. Phys.* **84,** 993–998 (1998).
11. T. Itoh and R. S. Rudokas, New method for computing the resonant frequencies of dielectric resonators, *IEEE Trans. Microwave Theory Technol.* **25,** 52–54 (1977).
12. S. Maj and M. Pospieszalski, A composite, multilayered cylindrical dielectric resonator, *in* "IEEE MTT-S Int. Microwave Symp. Dig.," pp. 190–192 (1984).
13. D. Kaifez and P. Guillon (Eds.), "Dielectric Resonators," Noble, Atlanta, GA (1998).
14. D. Maystre, P. Vincent, and J. C. Mage, Theoretical and experimental study of the resonant frequency of a cylindrical dielectric resonator, *IEEE Trans. Microwave Theory Technol.* **31,** 34–40 (1983).
15. K. H. Hellwege and A. M. Hellwege (Eds.), "Landolt-Boernstein New Series Numerical Data and Functional Relationships in Science and Technology, Group III, Vol. 9, Ferro- and Antiferroelectric Substances," Springer-Verlag, Berlin (1975).
16. P. G. Fajer, E. A. Fajer, J. J. Matta, and D. D. Thomas, Effect of the orientation of spin-labeled myosin heads in muscle fibers: A high-resolution study with deuterated spin labels, *Biochemistry* **29,** 5865–5871 (1990).
17. E. M. Ostap, V. A. Barnett, and D. D. Thomas, Resolution of three structural states of spin-labeled myosin in contracting muscle, *Biophys. J.* **69,** 177–188 (1995).
18. B. Salce, J. L. Gravil, and L. A. Boatner, Disorder and thermal transport in undoped $KTaO_3$, *J. Phys.: Condens. Matter* **6,** 4077–4092 (1994).
19. T. Scherban, A. S. Nowick, L. A. Boatner, and M. M. Abraham, Protons and other defects in Fe-doped $KTaO_3$, *Appl. Phys. A* **55,** 324–331 (1992).
20. W. Froncisz, T. Oles, and J. S. Hyde, Q-band loop-gap resonator, *Rev. Sci. Instrum.* **57,** 1095–1099 (1986).